Convergence of the multimode quantum Rabi model of circuit quantum electrodynamics

Gely, Mario F.; Parra-Rodriguez, Adrian; Bothner, Daniel; Blanter, Ya M.; Bosman, Sal J.; Solano, Enrique; Steele, Gary A.

Important note
To cite this publication, please use the final published version (if applicable).
Please check the document version above.

Convergence of the multimode quantum Rabi model of circuit quantum electrodynamics

Mario F. Gely,[1] Adrian Parra-Rodriguez,[2] Daniel Bothner,[1] Ya. M. Blanter,[1] Sal J. Bosman,[1]
Enrique Solano,[2,3] and Gary A. Steele[1]

[1]*Kavli Institute of NanoScience, Delft University of Technology, P.O. Box 5046, 2600 GA, Delft, The Netherlands*
[2]*Department of Physical Chemistry, University of the Basque Country UPV/EHU, Apartado 644, 48080 Bilbao, Spain*
[3]*IKERBASQUE, Basque Foundation for Science, Maria Diaz de Haro 3, 48013 Bilbao, Spain*

Circuit quantum electrodynamics (QED) studies the interaction of artificial atoms, open transmission lines, and electromagnetic resonators fabricated from superconducting electronics. While the theory of an artificial atom coupled to one mode of a resonator is well studied, considering multiple modes leads to divergences which are not well understood. Here, we introduce a first-principles model of a multimode resonator coupled to a Josephson junction atom. Studying the model in the absence of any cutoff, in which the coupling rate to mode number n scales as $\sqrt{n}$ for n up to ∞, we find that quantities such as the Lamb shift do not diverge due to a natural rescaling of the bare atomic parameters that arises directly from the circuit analysis. Introducing a cutoff in the coupling from a nonzero capacitance of the Josephson junction, we provide a physical interpretation of the decoupling of higher modes in the context of circuit analysis. In addition to explaining the convergence of the quantum Rabi model with no cutoff, our work also provides a useful framework for analyzing the ultrastrong coupling regime of a multimode circuit QED.

Quantum electrodynamics (QED) explores one of the most fundamental interactions in nature, that of light and matter. In a typical cavity QED scenario, an individual atom interacts through its dipole moment with the electric field of cavity modes, as described by the Rabi model [1] and depicted in Fig. 1(a). One consequence of this interaction is the Lamb shift of the atomic transition frequencies [2,3]. Early attempts at calculating this shift led to the first shortcomings of QED theory, mainly, that the transition energies of the atom diverge as the infinite number of electromagnetic modes are considered. Efforts to address these issues gave birth to renormalization theory [4]. Akin to cavity QED is the field of circuit QED [5], where artificial atoms such as anharmonic superconducting LC circuits couple to the modes of a waveguide resonator or an open transmission line. Such systems allow the study of a wealth of quantum effects [6,7] and are one of the most promising platforms for the realization of quantum processors [8–10]. Despite experimental successes, "ad hoc" multimode extensions of the Rabi model suffer from divergences when considering the limit of infinite modes in a waveguide resonator [11,12].

Aware of this problem, Nigg *et al.* [13,14] and Solgun *et al.* [15] developed the method of black-box quantization to obtain effective Hamiltonians with higher predictive power. While a practical tool for weakly anharmonic systems, this method was not designed for systems with strong anharmonicity, such as a Cooper pair box [16]. Furthermore, in applying the black-box procedure, the form of the quantum Rabi Hamiltonian is not preserved, and while it gives the correct energy spectrum, it is not clear how to identify and connect it to a coupling rate between the two bipartite systems. Doing so, it is no longer possible to directly identify which parts of the Rabi interaction lead to certain energy shifts of bare quantities, such as the Bloch-Siegert shift, highly relevant for studying the physics of ultrastrongly coupled (USC) systems [17,18].

In this paper, we derive a first-principles Hamiltonian model addressing these issues. This Hamiltonian is expressed in the basis of the uncoupled resonator modes and the atom, is valid for arbitrary atomic anharmonicities, and allows us to understand why previous attempts at extending the Rabi Hamiltonian have failed. The presence or not of a Josephson capacitance C_J in our study leads to two important results. First, in the limit $C_J \to 0$, the coupling rates follow a square-root increase up to an infinite number of modes. Without introducing a cutoff in the number of coupled modes, we show that a first-principles analysis of the quantum circuit leads to convergence of the energy spectrum. The $C_J = 0$ limit also highlights a natural renormalization of Hamiltonian parameters, arising from the circuit analysis, which is essential to understanding how to reach correct multimode extensions of the Rabi model. Second, we study the experimentally relevant case $C_J > 0$, which introduces a cutoff that suppresses the coupling to higher modes [19–21]. In particular, we provide an analysis of this regime and discuss the physics of this cutoff in the context of a lumped element circuit model. This results in a useful tool for studying multimode circuit QED in the framework of the Rabi Hamiltonian, or for studying strongly anharmonic regimes, out of reach of the black-box quantization method. This model was indispensable in extracting the Bloch-Siegert shift in the experiment of Ref. [18], where a naive extension of the Rabi model would predict a Lamb shift of more than 3 times the atomic frequency due to 35 participating modes before any physically motivated cutoff, such as the qubit's physical size or the junction capacitance, becomes relevant.

The circuit QED system studied in this work is an artificial atom (AA) formed from an anharmonic LC oscillator [16], capacitively coupled to a quarter-wave ($\lambda/4$) transmission line resonator [22] as depicted in Fig. 1(b). The AA is a superconducting island connected to ground through a Josephson junction characterized by its Josephson energy E_J. It has a capacitance to ground C_J and is coupled to the voltage antinode of the resonator, with characteristic impedance Z_0 and fundamental mode frequency $\omega_0/2\pi$, through a
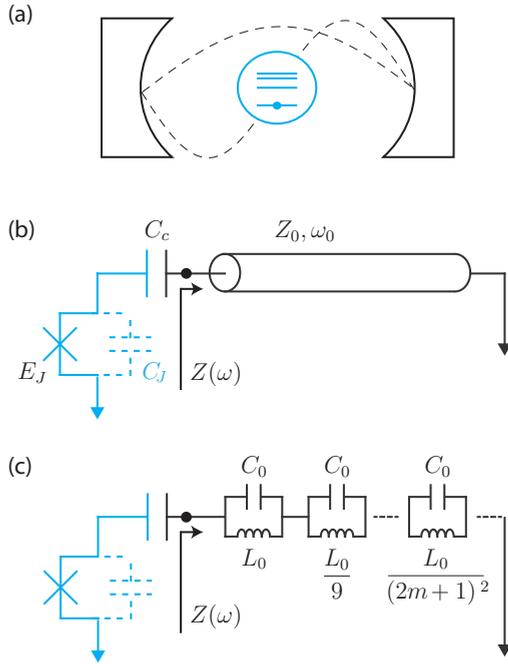
FIG. 1. (a) Schematic representation of cavity QED: A multilevel atom (in blue) coupled to the electromagnetic cavity modes (dashed black lines). (b) Circuit QED example covered in this work: A Josephson junction anharmonic LC oscillator, or "artificial atom," coupled to modes of a transmission line. (c) Lumped element equivalent of (b).

capacitance C_c. The Josephson junction acts as a nonlinear inductor, providing a source of single-photon anharmonicity in the oscillations of current flowing through it. In order to clearly illustrate the most novel aspect of our model, the renormalization of the charging energy, we first consider the case $C_J = 0$. Despite the absence of a cutoff in the number of coupled modes in this case, we find that the energy spectrum still converges. The case of $C_J > 0$ is discussed at the end of this article and in detail in the Supplemental Material [23].

Circuit Hamiltonian. We consider a Hamiltonian in which each uncoupled harmonic mode of the resonator, with resonance frequency ω_m and annihilation operator $\hat{a}_m$, is coupled to the transition between the bare atomic states $|i\rangle$, $|j\rangle$ with energies $\hbar\epsilon_i$, $\hbar\epsilon_j$ through a coupling strength $\hbar g_{m,i,j}$ [24,25]. We derive such a Hamiltonian by constructing a lumped element equivalent circuit, or Foster decomposition, of the transmission line resonator as represented in Fig. 1(c). The input impedance of a shorted transmission line, at a distance $\lambda/4$ from the short, $Z(\omega) = i Z_0 \tan[\pi\omega/(2\omega_0)]$, is equal to that of an infinite number of parallel LC resonators with capacitances $C_0 = \pi/(4\omega_0 Z_0)$ and inductances $L_m = 4Z_0/[(2m+1)^2\pi\omega_0]$. In order to consider a finite number of modes M in the model, one replaces the $m \geqslant M$ LC circuits in Fig. 1(c) by a short circuit to ground. This removes the $m \geqslant M$ resonances in the resonator input impedance $Z(\omega)$ with little effect on $Z(\omega)$ for $\omega \ll \omega_M$. The focus of this paper is on the evolution of the Hamiltonian parameters as a function of this system size M and the consequences on the energy spectrum. Using the tools of circuit quantization [26], we obtain as the

Hamiltonian of the system [23],

$$\hat{H}^{(M)} = \sum_i \hbar\epsilon_i^{(M)} |i\rangle^{(M)} \langle i|^{(M)} + \sum_{m=0}^{m<M} \hbar\omega_m \hat{a}_m^\dagger \hat{a}_m$$
$$+ \sum_{i,j} \sum_{m=0}^{m<M} \hbar g_{m,i,j}^{(M)} |i\rangle^{(M)} \langle j|^{(M)} (\hat{a}_m + \hat{a}_m^\dagger). \quad (1)$$

The eigenfrequencies of the higher resonator modes ω_m are related to those of the fundamental mode through $\omega_m = (2m+1)\omega_0$. The coupling strength $\hbar g_{m,i,j}^{(M)} = 2eV_{\text{zpf},m} \langle i|^{(M)} \hat{N}_J |j\rangle^{(M)}$ scales with the square root of the mode number m through the zero-point voltage fluctuations of the mth mode $V_{\text{zpf},m} = \sqrt{2m+1}\sqrt{\hbar\omega_0/2C_0}$. Since we will concentrate on the frequency and coupling of the first atomic transition $|g\rangle \rightarrow |e\rangle$, we use the shorthand $\omega_a^{(M)} = \epsilon_e - \epsilon_g$ and $g_m^{(M)} = g_{m,g,e}^{(M)}$ throughout this paper.

The (bare) AA eigenstates $|i\rangle^{(M)}$ and energies $\hbar\epsilon_i^{(M)}$ in Eq. (1) are those that diagonalize the Hamiltonian,

$$\hat{H}_{\text{AA}}^{(M)} = 4E_C^{(M)} \hat{N}_J - E_J \cos(\hat{\delta}). \quad (2)$$

Here $\hat{N}_J$ is the quantum number of Cooper pairs on the island conjugate to $\hat{\delta}$ the superconducting phase difference across the junction, and $E_C^{(M)}$ is the charging energy of the island. This choice of the decomposition of the Hamiltonian is one in which the bare atom corresponds to purely anharmonic degrees of freedom (currents flowing only through the junction) and the bare cavity to purely harmonic degrees of freedom (currents flowing only through the linear cavity inductors).

The crucial consequence of quantizing our model is a renormalization of the parameters of the Hamiltonian as modes are added. In particular, the charging energy $E_C^{(M)}$ of the (bare) AA depends explicitly on the number of modes included in the equivalent circuit,

$$E_C^{(M)} = \frac{e^2}{2} \frac{C_0 + MC_c}{C_0 C_c}, \quad (3)$$

as reported previously in the case of multiple atoms coupled to a single mode [27], or in the context of metallic dots coupled to a resonator [28]. For the case of $M \rightarrow \infty$ with $C_J = 0$, the charging energy of the bare atom diverges. This divergence arises from the definition of the bare atom as current oscillations flowing only through the junction. As $M \rightarrow \infty$, the impedance path through only the series capacitors of the resonator equivalent circuit diverges. Charge from currents through the junction can no longer oscillate on C_c and $\omega_a^{(M)}$ diverges. For the case of $M = 1$ and $C_c \ll C_0$, Eq. (3) simplifies to the standard definition of the charging energy $E_C = e^2/2C_c$ [16]. With $M > 1$, we will see that a more complex picture emerges.

Renormalization of the atomic parameters. In Fig. 2, we explore the renormalization of the parameters of our model as the number of modes M is increased. Through the change in charging energy, both the eigenstates $|i\rangle^{(M)}$ and coupling strengths $g_m^{(M)}$ depend on M. For a fixed number of modes M, the coupling $g_m^{(M)}$ of the atom to mode m scales with the square root of the mode number m: $g_m^{(M)} = g_0^{(M)}\sqrt{2m+1}$. From this coupling, each mode will induce a Lamb shift of the atomic energy
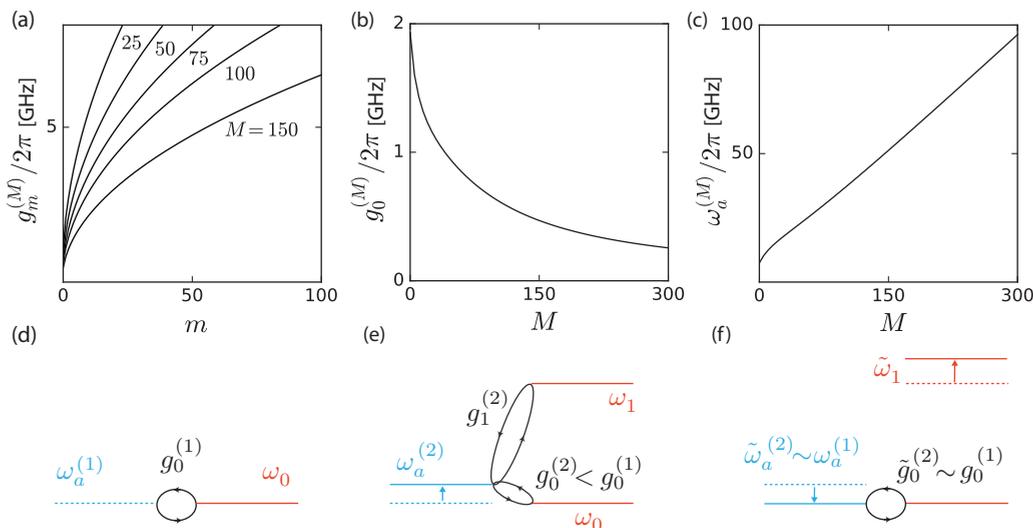
FIG. 2. Renormalization of the Hamiltonian parameters and dressing of the atom by higher modes. For the plots, we choose $\omega_0/2\pi = 10$ GHz, $Z_0 = 50$ Ω, $C_c = 50$ fF, and $E_J/h = 20$ GHz. Although this places the AA in the transmon limit, we note that the scaling shown in the figure is exact for all regimes, including the Cooper pair box limit. (a) Coupling of the ground to first excited-state transition of the atom $|g\rangle \rightarrow |e\rangle$ to the resonator modes as a function of the mode number m, $\hbar g_m^{(M)} = \sqrt{2m+1}V_{\mathrm{zpf},0}2e\langle g|^{(M)}\hat{N}_J|e\rangle^{(M)}$, for different values of M. The M dependence of the coupling is detailed in (b). (b), (c) Renormalization of the coupling strength and the atomic frequency through the change in charging energy $E_C^{(M)}$ as a function of M. For large M, the coupling diminishes with $1/M$ and the atomic frequency increases linearly with M. (d)–(f) Schematic energy diagrams of the renormalization procedure in the case of the atom and fundamental mode at resonance. (a) $M = 1$ and (b) $M = 2$. Adding a mode shifts the bare atomic energy upwards and changes the values of the couplings. (f) Dressing the atom with the second mode results in a dressed atomic state with atomic frequency and coupling to the $m = 1$ mode close to that of the $M = 1$ model.

$\chi_m \simeq -2(g_m^{(M)})^2/\omega_m = -2(g_0^{(M)})^2/\omega_0$, a formula valid in the transmon regime when ω_m is much larger than the bare atomic frequency. With the typical assumption of coupling and bare atomic frequency independent of M, summing the Lamb shifts of every mode would lead to diverging values of the dressed atomic frequencies. This leads to the divergences found in typical multimode extensions of the quantum Rabi model.

In the model presented here, however, we find that the full quantization of the lumped-element circuit leads to a Hamiltonian in which both the bare atomic frequency ω_a and the couplings to the modes g_m are explicitly dependent on the number of modes M included in the model. As the number of modes M in the model increases, the bare atomic couplings $g_m^{(M)}$ are suppressed [Figs. 2(a) and 2(b)], and the bare atomic frequency $\omega_a^{(M)}$ increases [Fig. 2(c)], diverging for an infinite number of modes. As we will see, however, convergence is obtained in the dressed transition energy of the atom when including the Lamb shift from higher modes of the resonator.

As an illustration of how renormalization in our model leads to convergence of the spectrum, let us consider the case shown in Figs. 2(d)–2(e) in which the fundamental mode is resonant with the atomic frequency $\omega_a^{(1)}$ when $M = 1$ [Fig. 2(d)]. Including an additional mode with frequency ω_1 will lead to an upward shift of the bare atomic transition $\omega_a^{(1)} \rightarrow \omega_a^{(2)} > \omega_a^{(1)}$ and a change of the coupling $g_0^{(1)} \rightarrow g_0^{(2)} < g_0^{(1)}$ through the renormalization of the charging energy [Fig. 2(e)]. Diagonalizing the subsystem of the atom and mode 1 in our model, the transition energy of the atom is shifted down again near resonance with the fundamental mode $\omega_a^{(2)} \rightarrow \tilde{\omega}_a^{(2)} \approx \omega_a^{(1)}$ by the dispersive shift, and the coupling of the atomic transition to the fundamental mode is increased

$g_0^{(2)} \rightarrow \tilde{g}_0^{(2)} \approx g_0^{(1)}$ [Fig. 2(f)]. In this way, the resulting vacuum Rabi splitting of the fundamental mode is found to be similar to that of the $M = 1$ model, despite the decrease in the bare coupling rates $g_0^{(2)}$.

Note that in our model, the value of $E_J/E_C^{(M)}$ of the bare atom, which determines its anharmonicity [16], is also a function of M. It would seem that in the limit $M \rightarrow \infty$, the bare atom would be deep in the Cooper pair box limit. However, including the hybridization with the cavity, the low-energy sector of $\hat{H}^{(M+1)}$ is well approximated by a model with M modes where the charging energy is not $E_C^{(M)}$ but

$$\tilde{E}_C^{(M)} = E_C^{(M+1)} - \hbar(\bar{g}_M^{(M+1)})^2/4\omega_M , \qquad (4)$$

where $\bar{g}_m^{(M)}$ is the coupling constant without the dipole moment $\langle i|^M \hat{N}_J|j\rangle^M$. For this to hold, $\hbar\omega_M$ must be larger than the characteristic energy of the low-energy sector of $\hat{H}^{(M)}$. In this case, the vacuum of the $(M+1)$th mode, shifted by $(\bar{g}_M^{(M+1)}/\omega_M)\hat{N}_J$, is a good variational choice for the low-lying energy sector of $\hat{H}^{(M+1)}$. In this subspace, the effective Hamiltonian is of the same form as $\hat{H}^{(M)}$, but with charging energy $\tilde{E}_C^{(M)}$ [23]. This result matches with the zeroth order of a Schrieffer-Wolff approximation [29,30]. We can iterate this procedure to a mode L. For $M \rightarrow \infty$, an effective Hamiltonian with L modes will have a finite charging energy,

$$\tilde{E}_C^{(L)} = \lim_{M \rightarrow \infty} E_C^{(M)} - \sum_{m \geqslant L}^{M} \hbar(\bar{g}_m^{(M)})^2/4\omega_m. \qquad (5)$$

The interaction with higher modes therefore modifies the charging energy of the dressed atom, leading to a convergence
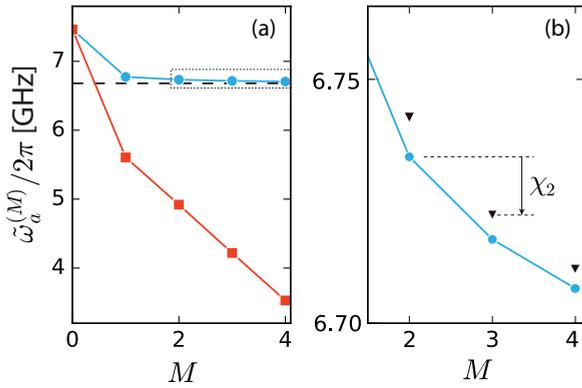
FIG. 3. Calculated spectrum as a function of the number of modes M included in the model. (a) Dots (squares) correspond to a diagonalization of the circuit (non-)renormalized extended-Rabi model. The frequency obtained by black-box quantization of the circuit Fig. 1(b) (dashed line) provides a point of reference corresponding to the case when all modes are included. (b) Zoom of dashed box in (a). Triangles show the prediction based on a first-order classical approximation of the Lamb shift: $\chi_M = \tilde{\omega}_a^{(M+1)} - \tilde{\omega}_a^{(M)} \simeq -2[(g_M^{(0)})^2/\omega_M][(\omega_a^{(0)})^2/\omega_M^2]$ [23].

of the atomic anharmonicity as well. This formula applies for all values of C_J, but for $C_J = 0$, we have $\tilde{E}_C^{(M)} = E_C^{(M)}$, i.e., the dressing from higher modes exactly compensates the renormalization of the charging energy.

In order to illustrate the effectiveness of this renormalization, in Fig. 3 we compare a diagonalization of Hamiltonian (1) to a nonrenormalized multimode extension of the quantum Rabi model, implemented by removing the M dependence of the charging energy $E_C^{(M)} \rightarrow e^2/(2C_c)$. The dashed line indicates the result of the black-box quantization (BB) method [13] as a point of reference. The calculations are performed using the same physical parameters as in Fig. 2. Compared to the nonrenormalized model, which diverges linearly, a diagonalization of the first-principles Hamiltonian (1) converges towards the value expected from BB.

It is also interesting to note that the corrections from our model are nonperturbative: perturbation theory fails to give a value for the Lamb shift resulting from including an extra mode. Using a circuit analysis of coupled LC oscillators (see [23]), in the transmon regime, $E_J \gg E_C^{(M)}$, we find an estimate of the shift in the dressed AA energy when including an additional mode in the model given by $\chi_m \simeq -2(g_m^2/\omega_m)(\tilde{\omega}_a^2/\omega_m^2)$. This formula can be used to estimate the number of relevant modes to include in a simulation and can be thought of as a replacement of the usual expression for the Lamb shift $\chi_m^{\text{Lamb}} \simeq -2g_m^2/\omega_m$.

Consequence of introducing a high-frequency cutoff. In a realistic system, higher modes will tend to decouple from the atom due to several coexisting physical mechanisms [12]. One such mechanism is the capacitance of the Josephson junction C_J. In particular, the capacitive loading of the cavity from the AA illustrated in the inset of Fig. 4 leads to a decreasing impedance to ground $Z_c(\omega) \simeq i(C_J + C_c)/\omega C_J C_c$ at the end of the resonator when $\omega \gg \omega_a$. When the mode frequencies become such that this impedance is lower than the characteristic impedance of the resonator $|Z_c(\omega)| \ll |Z_0|$,
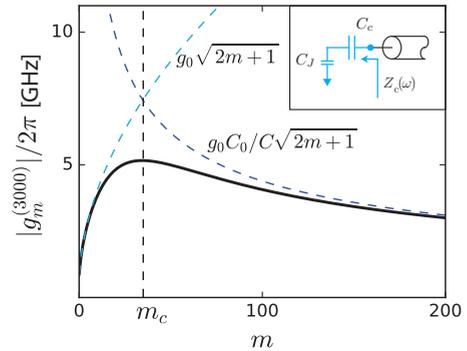
FIG. 4. High-frequency cutoff for $C_J \neq 0$. The capacitive loading at the left boundary of the resonator shown in the inset transforms this point from a voltage antinode to a voltage node for higher modes. The mode $m_c \simeq 35$ marks this transition. The solid line corresponds to the coupling strength as a function of the number of modes. With $C_J \neq 0$ the coupling strength converges to a nonzero value for large M; hence the choice $M = 3000$. Dashed lines: asymptotic values of the coupling, with $g_0 = g_0^{(M=3000)}$ and $C = C_c C_J/(C_c + C_J)$.

this voltage antinode of the resonator, to which the AA couples, becomes a voltage node, and the coupling vanishes. Additionally, the eigenfrequencies will span from those of a $\lambda/4$ resonator for the lower modes to those of a $\lambda/2$ resonator $\omega_m \rightarrow 2m\omega_0$ for the higher-lying modes.

This effect can be captured with the same quantization procedure applied to the circuit in Fig. 1(c) with $C_J \neq 0$ and is detailed in the Supplemental Material [23]. Mathematically, the cutoff in the coupling is due to a mode-mode coupling term of the form $\sum_{m=0}^{m<M} \sum_{m'=m+1}^{m'<M} G_{m,m'}^{(M)}(\hat{a}_m + \hat{a}_m^\dagger)(a_{m'} + a_{m'}^\dagger)$, which arises naturally from the circuit quantization. This is the equivalent of the A^2 term discussed in Refs. [19–21]. Diagonalizing the Hamiltonian of coupled resonator modes leads to decreasing zero-point voltage fluctuations of the modes at the coupling node. As shown in Fig. 4, with a capacitance to ground $C_J = 5$ fF close to the experimental parameters of Ref. [18], the expected cutoff occurs when $|Z_c(\omega_{m_c})| \simeq |Z_0|$, or equivalently, at the mode number $m_c \simeq (C_J + C_c)/2\omega_0 Z_0 C_J C_c$. This mechanism is accompanied by the appearance of an upper bound in the renormalized charging energy, such that Eq. (3) becomes

$$E_C^{(M)} = \frac{e^2}{2} \frac{C_0 + MC_c}{MC_c C_J + C_0(C_c + C_J)}, \qquad (6)$$

and $E_C^{(M)} \rightarrow e^2/2C_J$ for $M \rightarrow \infty$. We emphasize, however, that this cutoff is not a necessary condition for the convergence of the energy spectrum: the model described above with $C_J = 0$ converges even in the absence of such a cutoff. This is to be contrasted with typical models of (natural) atoms coupled to cavity modes where high-frequency cutoffs must be imposed to obtain finite predictions [31]. It would be interesting to study if the ideas developed in this work apply to such systems.

Conclusion. We have developed a first-principles multimode quantum Rabi model of circuit QED from a compact lumped element equivalent circuit. Using this formulation, we derived the convergence of quantities such as the Lamb shift in

the absence of any high-frequency cutoff, arising from a natural renormalization of the Hamiltonian parameters as modes are added. We also study the implications of a finite junction capacitance, which introduces a cutoff in the coupling to high-frequency modes but does not change the renormalization that occurs when additional modes are included in the circuit. For both cases with and without a junction capacitance, we show that when constructing a quantum Rabi model from this compact lumped element equivalent circuit it is crucial to include this renormalization to get correct Hamiltonian parameters from the values of the circuit elements. This work provides a useful framework for an intuitive understanding and modeling of experiments in the multimode ultrastrong coupling regime. This formulation of the multimode quantum Rabi model in the context of circuits hints at an intuitive picture on how this renormalization can arise physically, and it suggests the study of how this proposed physical picture could be applied to other problems in quantum field theory.

Note added. After we finished this manuscript, we became aware of Ref. [32], which arrives at similar conclusions as the last section of this article but through a different approach.

[1] I. I. Rabi, Phys. Rev. **49**, 324 (1936).

[2] W. E. Lamb, Jr. and R. C. Retherford, Phys. Rev. **72**, 241 (1947).

[3] D. J. Heinzen, Phys. Rev. Lett. **59**, 2623 (1988).

[4] H. A. Bethe, Phys. Rev. **72**, 339 (1947).

[5] A. Wallraff, D. Schuster, A. Blais, L. Frunzio, R. Huang, J. Majer, S. Kumar, S. Girvin, and R. J. Schoelkopf, Nature (London) **431**, 162 (2004).

[6] D. I. Schuster, A. A. Houck, J. A. Schreier, A. Wallraff, J. M. Gambetta, A. Blais, L. Frunzio, J. Majer, B. Johnson, M. H. Devoret, S. M. Girvin, and R. J. Schoelkopf, Nature (London) **445**, 515 (2007).

[7] L. S. Bishop, J. M. Chow, J. Koch, A. A. Houck, M. H. Devoret, E. Thuneberg, S. M. Girvin, and R. J. Schoelkopf, Nat. Phys. **5**, 105 (2009).

[8] M. Takita, A. D. Córcoles, E. Magesan, B. Abdo, M. Brink, A. Cross, J. M. Chow, and J. M. Gambetta, Phys. Rev. Lett. **117**, 210505 (2016).

[9] J. Kelly, R. Barends, A. G. Fowler, A. Megrant, E. Jeffrey, T. C. White, D. Sank, J. Y. Mutus, B. Campbell, Y. Chen, Z. Chen, B. Chiaro, A. Dunsworth, I.-C. Hoi, C. Neill, P. J. J. O 'malley, C. Quintana, P. Roushan, A. Vainsencher, J. Wenner, A. N. Cleland, and J. M. Martinis, Nature (London) **519**, 66 (2015).

[10] D. Ristè, S. Poletto, M.-Z. Huang, A. Bruno, V. Vesterinen, O.-P. Saira, and L. DiCarlo, Nat. Commun. **6**, 6983 (2015).

[11] A. A. Houck, J. A. Schreier, B. R. Johnson, J. M. Chow, J. Koch, J. M. Gambetta, D. I. Schuster, L. Frunzio, M. H. Devoret, S. M. Girvin, and R. J. Schoelkopf, Phys. Rev. Lett. **101**, 080502 (2008).

[12] S. Filipp, M. Göppl, J. M. Fink, M. Baur, R. Bianchetti, L. Steffen, and A. Wallraff, Phys. Rev. A **83**, 063827 (2011).

[13] S. E. Nigg, H. Paik, B. Vlastakis, G. Kirchmair, S. Shankar, L. Frunzio, M. H. Devoret, R. J. Schoelkopf, and S. M. Girvin, Phys. Rev. Lett. **108**, 240502 (2012).

[14] S. M. Girvin, in *Circuit QED: Superconducting Qubits Coupled to Microwave Photons*, Proceedings of the Les Houches Summer School Vol. 96 (Oxford University Press, New York, 2014).

[15] F. Solgun, D. W. Abraham, and D. P. DiVincenzo, Phys. Rev. B **90**, 134504 (2014).

[16] J. Koch, T. M. Yu, J. Gambetta, A. A. Houck, D. I. Schuster, J. Majer, A. Blais, M. H. Devoret, S. M. Girvin, and R. J. Schoelkopf, Phys. Rev. A **76**, 042319 (2007).

[17] P. Forn-Díaz, J. Lisenfeld, D. Marcos, J. J. García-Ripoll, E. Solano, C. J. P. M. Harmans, and J. E. Mooij, Phys. Rev. Lett. **105**, 237001 (2010).

[18] S. J. Bosman, M. F. Gely, V. Singh, A. Bruno, D. Bothner, and G. A. Steele, arXiv:1704.06208.

[19] S. De Liberato, Phys. Rev. Lett. **112**, 016401 (2014).

[20] J. J. García-Ripoll, B. Peropadre, and S. De Liberato, Sci. Rep. **5**, 16055 (2015).

[21] M. Malekakhlagh and H. E. Türeci, Phys. Rev. A **93**, 012120 (2016).

[22] D. M. Pozar, *Microwave Engineering* (John Wiley & Sons, New York, 2009).

[23] See Supplemental Material at http://link.aps.org/supplemental/10.1103/PhysRevB.95.245115 for a detailed derivation of the circuit Hamiltonians and its convergence as well as numerical methods.

[24] G. Zhu, D. G. Ferguson, V. E. Manucharyan, and J. Koch, Phys. Rev. B **87**, 024510 (2013).

[25] N. M. Sundaresan, Y. Liu, D. Sadri, L. J. Szocs, D. L. Underwood, M. Malekakhlagh, H. E. Tureci, and A. A. Houck, Phys. Rev. X **5**, 021035 (2015).

[26] M. H. Devoret, in *Quantum Fluctuations in Electrical Circuits (Les Houches Session LXIII)*, edited by S. Reynaud, E. Giacobino, and J. Zinn-Justin (Elsevier, New York, 1997).

[27] T. Jaako, Z.-L. Xiang, J. J. Garcia-Ripoll, and P. Rabl, Phys. Rev. A **94**, 033850 (2016).

[28] C. Bergenfeldt and P. Samuelsson, Phys. Rev. B **85**, 045446 (2012).

[29] J. R. Schrieffer and P. A. Wolff, Phys. Rev. **149**, 491 (1966).

[30] S. Bravyi, D. P. DiVincenzo, and D. Loss, Ann. Phys. (NY) **326**, 2793 (2011).

[31] L. Mandel and E. Wolf, *Optical Coherence and Quantum Optics* (Cambridge University Press, Cambridge, 1995).

[32] M. Malekakhlagh, A. Petrescu, and H. E. Türeci, arXiv:1701.07935v2.